Inorg. Chem. **2005**, *44*, 8715–8722

A New Coordination Mode of the Photometric Reagent Glyoxalbis(2-hydroxyanil) (H_2gbha): Bis-Bidentate Bridging by gbha^{2-} in the Redox Series $\{(\mu\text{-gbha})[Ru(acac)_2]_2\}^n$ ($n = -2, -1, 0, +1, +2$), Including a Radical-Bridged Diruthenium(III) and a Ru^{III}/Ru^{IV} Intermediate

Sanjib Kar,[†] Biprajit Sarkar,[‡] Sandeep Ghumaan,[†] Dipankar Roy,[†] Francisco A. Urbanos,[||] Jan Fiedler,[§] Raghavan B. Sunoj,*[,†] Reyes Jimenez-Aparicio,*[,||] Wolfgang Kaim,*[,‡] and Goutam Kumar Lahiri*[,†]

Department of Chemistry, Indian Institute of Technology—Bombay, Powai, Mumbai 400076, India, Institut für Anorganische Chemie, Universität Stuttgart, Pfaffenwaldring 55, D-70550 Stuttgart, Germany, J. Heyrovsky Institute of Physical Chemistry, Academy of Sciences of the Czech Republic, Dolejškova 3, CZ-18223 Prague, Czech Republic, and Departamento de Química Inorgánica, Facultad de Ciencias Químicas, Universidad Complutense, Ciudad Universitaria, E28040 Madrid, Spain

Received June 13, 2005

The bis-bidentate bridging function of gbha^{2-} with N,O$^-$/N,O$^-$ coordination was observed for the first time in the complex (μ-gbha)[Ru^{III}(acac)$_2$]$_2$ (**1**). Density functional theory calculations of **1** yield a triplet ground state with a large (ΔE > 6000 cm^{-1}) singlet–triplet gap. Intermolecular antiferromagnetic coupling was observed ($J \approx -5.3$ cm^{-1}) for the solid. Complex **1** undergoes two one-electron reduction and two one-electron oxidation steps; the five redox forms $\{(\mu\text{-gbha})[Ru(acac)_2]_2\}^n$ ($n = -2, -1, 0, +1, +2$) were characterized by UV–vis–NIR spectroelectrochemistry (NIR = near infrared). The paramagnetic intermediates were also investigated by electron paramagnetic resonance (EPR) spectroscopy. The monoanion with a comproportionation constant K_c of 2.7×10^8 does not exhibit an NIR band for a Ru^{III}/Ru^{II} mixed-valent situation; it is best described as a 1,4-diazabutadiene radical anion containing ligand gbha$^{\bullet 3-}$, which binds two ruthenium(III) centers. A Ru^{III}-type EPR spectrum with $g_1 = 2.27$, $g_2 = 2.21$, and $g_3 = 1.73$ is observed as a result of antiferromagnetic coupling between one Ru^{III} and the ligand radical. The EPR-active monocation ($K_c = 1.7 \times 10^6$) exhibits a broad ($\Delta\nu_{1/2} = 2600$ cm^{-1}) intervalence charge-transfer band at 1800 nm, indicating a valence-averaged $(Ru^{3.5})_2$ formulation (class III) with a tendency toward class II (borderline situation).

Introduction

Since the introduction of glyoxalbis(2-hydroxyanil) (H_2gbha) as a tetradentate chelate ligand in the deprotonated form gbha^{2-} (*s*-cis form) by Bayer and co-workers[1] in the 1950s, there have been several reports describing mononuclear complexes (L_nM)(gbha), with M = main group, transition metal, and actinide elements.[2,3] In particular, H_2gbha has been

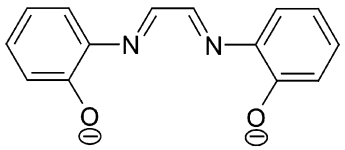

gbha^{2-}
s-cis

used as a photometric reagent in the analytical determination of Ca^{2+}.[3] However, if the central bond, in what may be alternatively described as 1,4-bis(2-phenolato)-1,4-diazabutadiene (= gbha^{2-}), adopts the *s*-trans instead of the *s*-cis

* Authors to whom correspondence should be addressed. E-mail: lahiri@chem.iitb.ac.in (G.K.L.), kaim@iac.uni-stuttgart.de (W.K.).
[†] Indian Institute of Technology—Bombay.
[‡] Universität Stuttgart.
[§] Academy of Sciences of the Czech Republic.
[||] Universidad Complutense, Ciudad Universitaria.

(1) (a) Bayer, E. *Angew. Chem.* **1957**, *69*, 107. (b) Bayer, E. *Angew. Chem.* **1959**, *71*, 426. (c) Bayer, E. *Chem. Ber.* **1957**, *90*, 2325. (d) Bayer, E. *Chem. Ber.* **1957**, *90*, 2785. (e) Bayer, E.; Schenk, G. *Chem. Ber.* **1960**, *93*, 1184. (f) Bayer, E. *Angew. Chem.* **1964**, *76*, 76; *Angew. Chem., Int. Ed. Engl.* **1964**, *3*, 325.

10.1021/ic050950r CCC: $30.25
Published on Web 10/19/2005

conformation, this ligand can function also as a π-conjugated bis-bidentate bridge, coordinating two metals each with one imine-N π-acceptor and one phenolato-O π-donor atom. Remarkably, such a case has not yet been described. In this

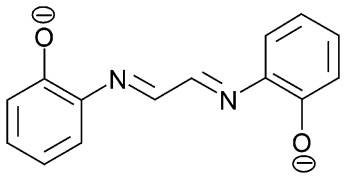

$gbha^{2-}$

s-trans

report, we present the first example using $[Ru(acac)_2]$ complex fragments ($acac^-$ = acetylacetonate = 2,4-pentanedionate). The compound was obtained in its diruthenium(III)-containing neutral form $\{(\mu\text{-gbha})[Ru(acac)_2]_2\}^n$ (n = 0), which was also subjected to density functional theory (DFT) calculations and susceptibility measurements. Since cyclic voltammetry revealed two well-separated one-electron reduction and two one-electron oxidation steps, all accessible redox forms (n = −2, −1, 0, +1, +2) were characterized by UV−vis−NIR spectroelectrochemistry (NIR = near infrared); the paramagnetic intermediates were investigated by electron paramagnetic resonance (EPR) spectroscopy.

Results and Discussion

The paramagnetic diruthenium(III) complex $(acac)_2Ru^{III}(\mu\text{-gbha})Ru^{III}(acac)_2$ (**1**) was synthesized via the reaction of the metal precursor $Ru(acac)_2(CH_3CN)_2$ with glyoxalbis(2-hydroxyanil) (H_2gbha) in the presence of oxidizing air and CH_3COONa as a base in refluxing ethanol. The metalation aspects of H_2gbha have been confined only to the mononuclear level so far, with the *s*-cis form of tetradentate $gbha^{2-}$ coordinated to one metal ion via the $^-$O,N/N,O^- donors.[1−3] The dinucleating bridging feature of the *s*-trans form of $gbha^{2-}$ has been evidenced for the first time in **1**, where it binds two ruthenium ions by using the terminal $^-$O,N (phenolato oxygen and imine nitrogen) functions, leading to a double $Ru^{III}O_5N$ situation in combination with the $acac^-$ (acetylacetonato) ancillary ligands at each site of the bridge. Although the dinuclear complex **1** with three bidentate ligands around each metal center can, in principle, exist as pairs of enantiomers ($\Delta\Delta$, $\Lambda\Lambda$; C_2 symmetry) or as the meso form (Δ, Λ; C_s symmetry),[4] our careful preparatory thin-layer chromatography experiments confirmed the presence of only one form, either the meso or rac isomer. The Ru^{II} ion in the precursor $Ru(acac)_2(CH_3CN)_2$ has been oxidized to the Ru^{III} state in **1**, presumably by O_2. The presence of electron-rich O^- donors in the complex moiety destabilizes the ruthenium(II) state significantly, reflected by a low ruthenium(III)−ruthenium(II) potential of −0.51 V versus the saturated calomel electrode (SCE), which in turn facilitates the stabilization of Ru^{III} in **1** under aerobic conditions.

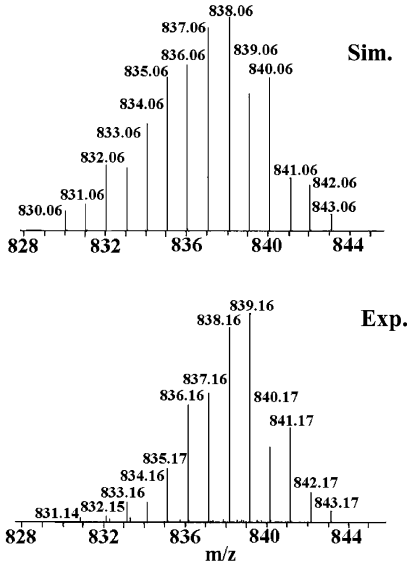

Figure 1. ESI mass spectra (simulated, top, and experimental, bottom) of **1** in CH_2Cl_2.

The identity of **1** is authenticated by an elemental analysis (see Experimental Section) and by the electrospray mass spectral data (Figure 1). The observed ES+ signal is centered at an *m*/*z* value of 839.16, which corresponds to $\mathbf{1}^+$ (calculated mass: 838.06).

Complex **1** shows an exponential increase of the molar magnetic susceptibility from 300 to 2 K (Figure S1a, Supporting Information). The reciprocal magnetic susceptibility versus temperature follows the Curie−Weiss law below 30 K with $\theta = -6.1$ K but exhibits substantial deviation from linearity at higher temperatures (Figure S1b, Supporting Information). The observed magnetic moment of 3.79 μ_B at 298 K is higher than the spin-only magnetic moment expected for two low-spin Ru(III) centers in **1**. μ_{eff} decreases almost linearly down to 50 K; however, it falls sharply to 1.38 μ_B in the temperature range of 50−2 K.

The observed high μ_{eff} value for **1** at 298 K in comparison to spin-only values indicates the involvement of orbital contributions associated with the degenerate $^2T_{2g}$ ground state of the Ru^{III} ion. On the other hand, the low μ_{eff} at 2 K suggests the presence of inter- or intramolecular antiferromagnetic coupling between the Ru^{III} centers.[5,6]

(2) (a) Bandoli, G.; Clemente, D. A. *J. Chem. Soc., Dalton Trans.* **1975**, 612. (b) Benedix, R.; Dietz, F.; Hennig, H. *Inorg. Chim. Acta* **1988**, *147*, 179. (c) Bandoli, G.; Cattalini, L.; Clemente, D. A.; Vidali, M.; Vigato, P. A. *J. Chem. Soc., Chem. Commum.* **1972**, 344. (d) Majima, T.; Kawasaki, Y. *Bull. Chem. Soc. Jpn.* **1978**, *51*, 1893.

(3) Ferguson, E.; Vaughan, A.; Swale, J. *Clin. Chim. Acta* **1976**, *67*, 281.

(4) (a) Kar, S.; Sarkar, B.; Ghumaan, S.; Janardanan, D.; van Slageren, J.; Fiedler, J.; Puranik, V. G.; Sunoj, R. B.; Kaim, W.; Lahiri, G. K. *Chem. Eur. J.* **2005**, *11*, 4901. (b) Ghumaan, S.; Sarkar, B.; Patra, S.; Parimal, K.; van Slageren, J.; Fiedler, J.; Kaim, W.; Lahiri, G. K. *Dalton Trans.* **2005**, 706. (c) Sarkar, B.; Patra, S.; Fiedler, J.; Sunoj, R. B.; Janardanan, D.; Mobin, S. M.; Niemeyer, M.; Lahiri, G. K.; Kaim, W. *Angew. Chem., Int. Ed.* **2005**, *44*, 5655. (d) Chakraborty, S.; Laye, R. H.; Munshi, P.; Paul, R. L.; Ward, M. D.; Lahiri, G. K. *J. Chem. Soc., Dalton Trans.* **2002**, 2348. (e) Sarkar, B.; Laye, R. H.; Mondal, B.; Chakraborty, S.; Paul, R. L.; Jeffery, J. C.; Puranik, V. G.; Ward, M. D.; Lahiri, G. K. *J. Chem. Soc., Dalton Trans.* **2002**, 2097. (f) Chakraborty, S.; Laye, R. H.; Paul, R. L.; Gonnade, R. G.; Puranik, V. G.; Ward, M. D.; Lahiri, G. K. *J. Chem. Soc., Dalton Trans.* **2002**, 1172.

Thus, the magnetic data of **1** have been analyzed by using the model (eq 1) that considers spin−orbit coupling (λ), a Weiss constant (θ), and temperature-independent paramagnetism (TIP). The Hamiltonian $H = \lambda\hat{L}\hat{S}$, applied to the $^2T_{2g}$ ground term of Ru^{III} in a cubic field, and the resultant energy terms and coefficients included in the Van Vleck equation yield the susceptibility formula (eq 1) for a system with spin−orbit coupling.[7a] The average g value is assumed to be 2. Thus, the magnetic susceptibility of **1** corresponds to $2 \times \chi_M$.

$$\chi_M = \frac{N\beta^2}{3k(T-\theta)} \frac{8 + \left(\frac{3\lambda}{kT} - 8\right)\exp\left(-\frac{3\lambda}{2kT}\right)}{\frac{\lambda}{kT}\left[2 + \exp\left(-\frac{3\lambda}{2kT}\right)\right]} + \text{TIP} \quad (1)$$

In eq 1, N, β, λ, k, θ, and T have their usual meanings. A very good agreement between the experimental and calculated values of the magnetic moment as well as the molar magnetic susceptibility has been obtained for **1** using this model (eq 1; Figure S1, Supporting Information). The best fitting of the magnetic data gives $\lambda = -549$ cm^{-1}, $\theta = -3.85$ K, and TIP $= 5.9 \times 10^{-4}$ emu mol^{-1} with $\sigma^2 = 5.4 \times 10^{-5}$ [$\sigma^2 = \sum(\mu_{eff/calc} - \mu_{eff/exp})^2/\sum\mu_{eff/exp}{}^2$].

A J value of -5.37 cm^{-1}, obtained from the expression $\theta = 2JS(S+1)/3k$, confirms the existence of weak inter- or intramolecular antiferromagnetic coupling between the Ru^{III} centers in **1**.[8]

Although the use of a Weiss constant to take into account the existence of a weak ferro- or antiferromagnetic interaction is frequent when J is considerably lower than the spin−orbit coupling, the consideration of the molecular field approximation[7b] (eq 2) could be more appropriate.

$$\chi_M = \frac{\chi'_M}{1 - (2zJ/N2^2\beta^2)\chi'_M} + \text{TIP} \quad (2)$$

where χ'_M considers the spin−orbit coupling through the expression

$$\chi'_M = \frac{N\beta^2}{3kT} \frac{8 + \left(\frac{3\lambda}{kT} - 8\right)\exp\left(-\frac{3\lambda}{2kT}\right)}{\frac{\lambda}{kT}\left[2 + \exp\left(-\frac{3\lambda}{2kT}\right)\right]}$$

A fit of the magnetic moment and the susceptibility curves via eq 2 gives the parameters $\lambda = -526$ cm^{-1}, $J = -5.17$ cm^{-1}, and TIP $= 5.9 \times 10^{-4}$ emu mol^{-1} with $\sigma^2 = 6.8 \times 10^{-5}$ [$\sigma^2 = \sum(\mu_{eff/calc} - \mu_{eff/exp})^2/\sum\mu_{eff/exp}{}^2$]. Thus, both equations (eqs 1 and 2) lead to very similar magnetic parameters for **1**.

Although an intramolecular antiferromagnetic interaction between the Ru^{III} ions in **1** through the $gbha^{2-}$ ligand could be considered, the theoretical studies (cf. below) indicate that **1** has a triplet ground-state configuration. Moreover, the calculated large energy difference between the triplet and singlet states ($\Delta E > 6000$ cm^{-1}) suggests the absence of significant intramolecular magnetic interactions. As a consequence, the decrease of the magnetic moment with the temperature can be interpreted as an *intermolecular* antiferromagnetic interaction between adjacent molecules of **1** in the solid.

The calculated spin−orbit coupling constant of -526 cm^{-1} is somewhat lower than the values reported for monomeric Ru^{III} complexes such as *trans*-$[(acac)_2Ru(L)_2](ClO_4)$ (L = 2,2′-dipyridylamine; $\lambda = -690$ cm^{-1})[6a] or $[Ru(CN)_6]^{3-}$ ($\lambda = -880$ cm^{-1}).[6b] In general, λ values for low-spin Ru^{III} complexes vary between -700 and -1000 cm^{-1}. The low λ value for **1** can be explained by partial delocalization of the spins between the metal centers and the organic bridging ligand, which should diminish the role of the orbital moment. An extraordinarily low λ value of -100 cm^{-1} for the complex $[\{Ru(CH_3CN)_3[P(OMe)_3]_2\}_2(\mu\text{-}S_2)]^{3+}$ was explained in terms of spin delocalization between the metal and the ligands.[9]

Compound **1** exhibits a relatively weak axial EPR signal at 110 K in CH_2Cl_2 [g(perpendicular) = 2.21 and g(parallel) = 1.76; Figure 2a]. In agreement with susceptibility results, the intensity decreases at lower temperatures. Both the g anisotropy ($\Delta g = g_1 - g_3$) of 0.45 and the average g ($g_{av} = [(1/3)(g_1{}^2 + g_2{}^2 + g_3{}^2)]^{1/2}$) of 2.076 from EPR spectroscopy are indicative of a Ru^{III}-based spin.[10] The half-field EPR signal expected for a triplet state[11] was not observed under those conditions. The observation of very broad ^{1}H NMR features at room temperature in solution confirms the paramagnetism of **1**.

The triplet ground state of **1** is calculated to lie 6235 cm^{-1} lower than the lowest singlet state. The B3LYP/SDD,6-31G* optimized geometry of **1** in its triplet ground state is shown in Figure 3, and the calculated structural parameters are summarized in Table S1 (Supporting Information). The planarity of the bridging ligand $gbha^{2-}$ in **1** is evident from the optimized geometry as revealed by the torsional angle (N3−C7−C8−N4) of 179.97°. The intermetallic separation between the ruthenium(III) centers in **1** is calculated to be 6.441 Å. The calculated Ru^{III}−O^- (phenolato), Ru^{III}−O^- (acac), and Ru^{III}−N (imine) distances match reasonably well with those of the structurally characterized related molecules.[3,4,12,13]

(5) (a) Grillo, V. A.; Gahan, L. R.; Hanson, G. R.; Stranger, V.; Hambley, T. W.; Murray, K. S.; Moubaraki, B.; Cashion J. D. *J. Chem. Soc., Dalton Trans.* **1998**, 2341 (b) Bernhardt, P. V.; Comba, P.; Hambley, T. W.; Lawrance, G. A. *Inorg. Chem.* **1991**, *30*, 942.
(6) (a) Kar, S.; Chanda, N.; Mobin, S. M.; Urbanos, F. A.; Niemeyer, M.; Puranik, V. G.; Jimenez-Aparicio, R.; Lahiri, G. K. *Inorg. Chem.* **2005**, *44*, 1571. (b) Bendix, J.; Steenberg, P.; Sotofte, I. *Inorg. Chem.* **2003**, *42*, 4510.
(7) (a) Mabbs, F. E.; Machin, D. J. *Magnetism and Transition Metal Complexes;* Chapman and Hall Ltd: London, 1973; p 68. (b) O'Connor, C. J. *Prog. Inorg. Chem.* **1982**, *29*, 203.
(8) (a) Figgis, B. N.; Reynolds, P. A.; Murray, K. S. *Aust. J. Chem.* **1998**, *51*, 229. (b) Bernhard, P.; Stebler A.; Ludi, A. *Inorg. Chem.* **1984**, *23*, 2151.
(9) Matsumoto, K.; Matsumoto, T.; Kawano, M.; Ohnuki, H.; Shichi, Y.; Nishide, T.; Sato, T. *J. Am. Chem. Soc.* **1996**, *118*, 3597.
(10) Patra, S.; Sarkar, B.; Mobin, S. M.; Kaim, W.; Lahiri, G. K. *Inorg. Chem.* **2003**, *42*, 6469.
(11) Ghumaan, S.; Sarkar, B.; Patra, S.; van Slageren, J.; Fiedler, J.; Kaim, W.; Lahiri, G. K. *Inorg. Chem.* **2005**, *44*, 3210.

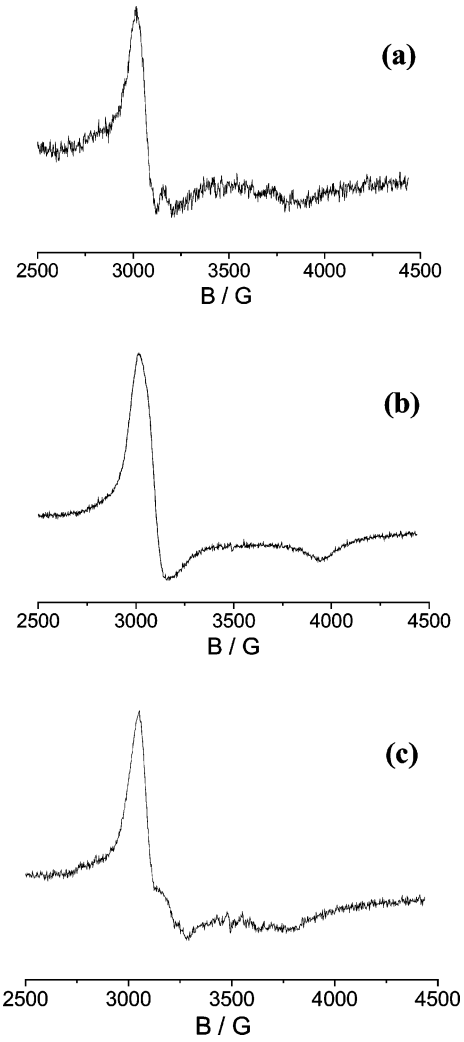

Figure 2. EPR spectra of (a) **1**, (b) $\mathbf{1}^-$, and (c) $\mathbf{1}^+$ in CH_2Cl_2/0.1 M Bu_4NPF_6 at 110 K.

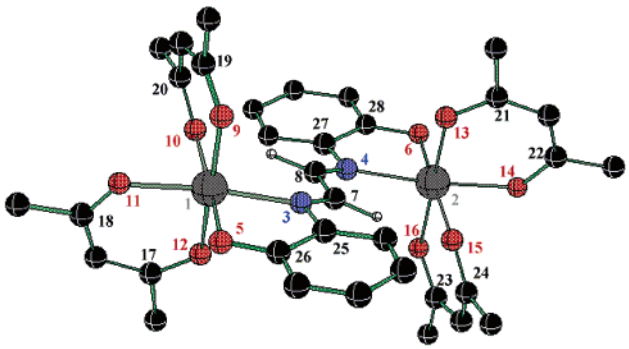

Figure 3. B3LYP/SDD,6-31G* optimized geometry for the triplet ground state of **1**.

The central C(7)−C(8) bond length in **1** is found to be 1.426 Å ,while the N(3)═C(7) and N(4)═C(8) distances are 1.312 Å. The C(7)−C(8) and N(3)═C(7) bond lengths calculated for the uncomplexed ligand $gbha^{2-}$ at the same level of theory were found to be 1.450 and 1.295 Å, respectively, suggesting a rather unperturbed ligand framework in **1**. An analysis of electron delocalization using the natural bond orbital method revealed the existence of $d\pi$(Ru)-to-π^*(N═C) back-donation in **1**, resulting in the increased N═C and shortened central C(7)−C(8) distances. Similar bond length variations arising as a result of complimentary orbital interactions have been reported previously.[14]

In contrast to the triplet ground state characterized by a relatively unperturbed, little-delocalized, and thus weakly metal−metal-coupling 1,4-diazabutadiene linker, the high-energy singlet state was calculated with almost averaged C−N and central C−C bonds at 1.362 and 1.376 Å, respectively. Obviously, spin−spin coupling requires a delocalized NCCN backbone with significant negative charges on the nitrogen donors, and as a consequence, the calculated Ru−N distance decreases from 2.097 (triplet) to 2.005 Å in the singlet state (Table S2 and Figure S2, Supporting Information).

Computed vertical excitation energies with the time-dependent density functional theory (TD-DFT) formalism on the B3LYP/SDD,6-31G* optimized geometry for **1** in its triplet ground state are summarized in Table 1. The nature of the excited states is assigned on the basis of the percent Kohn−Sham orbital contributions of the orbitals involved in the electronic transitions. On the basis of the predicted values for the oscillator strengths, it is found that the most intense long-wavelength transition occurs from a singly occupied molecular orbital (SOMO) to the lowest unoccupied molecular orbital (LUMO), assigned to a mixed metal−ligand [$d\pi$(Ru), 86%, and π(gbha), 14%] to ligand [π^*(gbha)] transition (MLLCT) (Figure 4). At 594 nm, the computed wavelength is comparable to the higher intensity absorption obtained experimentally, which lies at λ_{max} = 649 nm (Figure 5a; Table 2); the shoulders at 600 and 560 nm are attributed to vibrational splitting.

Complex **1** exhibits two one-electron reduction waves at $E_{298}°$/V (ΔE_p/mV), −0.51 (150) and −1.0 V (120 mV) versus SCE in CH_2Cl_2/0.1 M Et_4NClO_4; two one-electron oxidation waves occur at 0.78 (120) and 1.15 V (150 mV) (Figure 6). The comproportionation constants K_c [calculated using the equation $RT\ \ln K_c = nF(\Delta E)$[15]] for the odd-electron intermediates $\{(\mu\text{-gbha})[Ru(acac)_2]_2\}^-$ ($\mathbf{1}^-$) and $\{(\mu\text{-gbha})[Ru(acac)_2]_2\}^+$ ($\mathbf{1}^+$) amount to 2.7×10^8 and 1.7×10^6, respectively. Optically transparent thin-layer electrode (OTTLE) spectroelectrochemistry[16] in the UV−vis−NIR region (Figure 5; Table 2) was used to investigate the sites of electron transfer starting from the neutral complex (μ-$gbha^{2-}$)[$Ru^{III}(acac)_2]_2$ (**1**). In **1**, not only the trivalent ruthenium(III) centers can be oxidized and reduced but the

(12) (a) Lahiri, G. K.; Bhattacharya, S.; Mukherjee, M.; Mukherjee, A. K.; Chakravorty, A. *Inorg. Chem.* **1987**, *26*, 3359. (b) Bag, N.; Lahiri, G. K.; Bhattacharya, S.; Falvello, L. R.; Chakravorty, A. *Inorg. Chem.* **1988**, *27*, 4396. (c) Mondal, B.; Chakraborty, S.; Munshi, P.; Walawalkar, M. G.; Lahiri, G. K. *J. Chem. Soc., Dalton Trans.* **2000**, 2327. (d) Patra, S.; Mondal, B.; Sarkar, B.; Niemeyer, M.; Lahiri, G. K. *Inorg. Chem.* **2003**, *42*, 1322. (e) Kar, S.; Chanda, N.; Mobin, S. M.; Datta, A.; Urbanos, F. A.; Puranik, V. G.; Jimenez-Aparicio, R.; Lahiri, G. K. *Inorg. Chem.* **2004**, *43*, 4911.

(13) (a) Das, S.; Chakraborty, I.; Chakravorty, A. *Inorg. Chem.* **2003**, *42*, 6545. (b) Mondal, B.; Puranik, V. G.; Lahiri, G. K. *Inorg. Chem.* **2002**, *41*, 5831.

(14) Reed, A. E.; Schleyer, P. v. R. *J. Am. Chem. Soc.* **1990**, *112*, 1434.

(15) Robin, M. B.; Day, P. *Adv. Inorg. Chem. Radiochem.* **1967**, *10*, 247.

(16) Krejcik, M.; Danek, M.; Hartl, F. *J. Electroanal. Chem.* **1991**, *317*, 179.

Table 1. Selected List of Vertical Excitations[a] Computed at the TD-DFT/B3LYP//B3LYP/SDD,6-31G* Level for **1** in the Triplet Ground State

excitation energy[b] in cm^{-1}	oscillator strength	ϵ[c]	$\psi_o-\psi_v$[d,e,f]	type of transition
13 611 (734.7)	0.0339	2379	179 β [HOMO−4] → 184 β [LUMO] (0.57)[g]	dπ(Ru), π(phenolate) → π^*(gbha^{2-})
16 842 (593.8)	0.3041	21 347	185 α [HOMO] → 186 α [LUMO] (0.62)	dπ(Ru), π(gbha^{2-}) → π^*(gbha^{2-})
17 443 (573.3)	0.0188	1319	182 β [HOMO−1] → 185 β [LUMO+1] (0.75)	dπ(Ru), π(gbha^{2-}) → dπ(Ru)
18 310 (546.1)	0.0019	133	181 β [HOMO-2] → 184 β [LUMO] (0.53)	dπ(Ru) → π^*(gbha^{2-})
			181 β [HOMO-2] → 186 β [LUMO+2] (0.64)	dπ(Ru) → dπ(Ru), π^*(gbha^{2-})

[a] Calculations were done by employing an SDD basis set for Ru and the 6-31G* basis set for the other elements; triplet excitation energies. [b] Wavelengths in nm given in parentheses. [c] ϵ in M^{-1} cm^{-1}. [d] Occupied and virtual orbitals. [e] There are 185 singly occupied α orbitals and 183 singly occupied β orbitals. [f] All orbitals such as HOMO, HOMO −1, and HOMO − 2 are singly occupied molecular orbitals (SOMOs). [g] Transition coefficient.

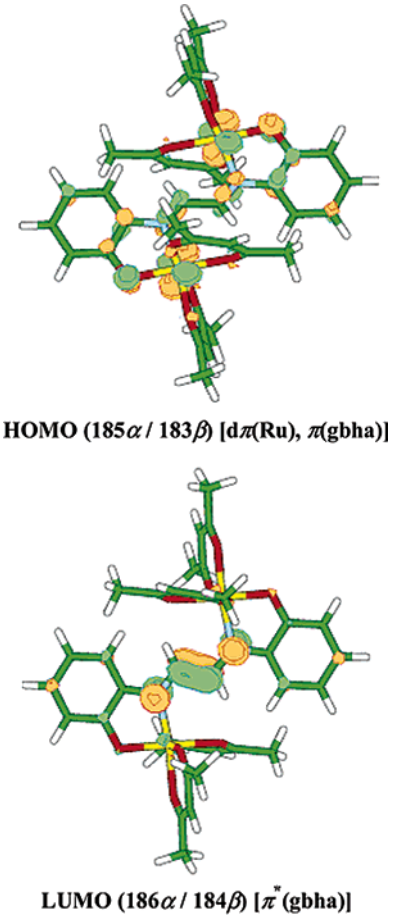

Figure 4. Kohn−Sham orbital contours of the HOMO [185α] and LUMO [186α] of **1** involved in the most intense long-wavelength transition.

"*noninnocent*" bridging ligand gbha^{2-} can, in principle, adopt five oxidation states, as indicated by the appropriate structures in Scheme 1.

Starting from the neutral complex **1** with its intense MLLCT band at 649 nm, the first reduction **1**$^-$ leads to a low-energy shift (735 nm) (Figure 5a), which is still more pronounced after filling up with another electron in the second reduction (828 nm) to **1**$^{2-}$ (Figure 5b). This spectral behavior and the absence of detectable absorption intensity in the NIR region in **1**$^-$ (Figure 5a) are less compatible with a Ru^{III}/Ru^{II} mixed-valent formulation, which would be expected to have an intervalence charge transfer (IVCT) band in the NIR region.[17] As a consequence, we favor a 1,4-diazabutadiene (α-diimine) centered reduction of the bridging ligand (see Schemes 1 and 2), in agreement with the π^*(gbha^{2-}) as LUMO; radical anions and dianions of free and, especially, coordinated 1,4-diazabutadienes have been well-established for more than 30 years.[13a,18] The EPR results obtained at 110 K for the intermediate are in agreement with an up/down/up three-spin[19] formulation of {(μ-gbha$^{\bullet 3-}$)-[Ru^{III}(acac)$_2$]$_2$}$^-$. Antiferromagnetic coupling between one Ru^{III} ion and the ligand radical leaves one $S = {}^1/_2$ metal center spin remaining, leading again to a Ru^{III}-type EPR spectrum with $g_1 = 2.27$, $g_2 = 2.21$, and $g_3 = 1.73$ (Figure 2b). The average g factor (g_{av}) and the g anisotropy (Δg) are 2.084 and 0.54, respectively.

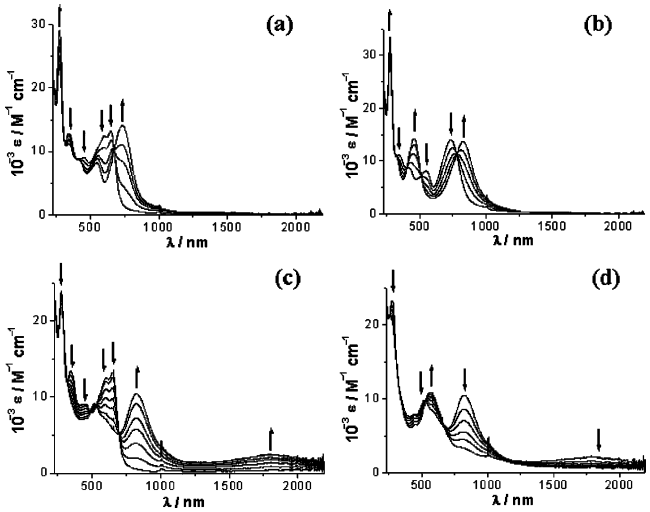

Figure 5. UV−vis−NIR spectroelectrochemistry of the conversions: (a) **1** → **1**$^-$, (b) **1** → **1**$^{2-}$, (c) **1** → **1**$^+$, and (d) **1** → **1**$^{2+}$ in CH_2Cl_2/0.1 M Bu_4NPF_6.

The high intensity of the EPR signal for **1**$^-$ in comparison to that for **1** (triplet) or **1**$^+$ (see below) indicates slow relaxation; otherwise, the g parameters are rather similar, as expected.

Similar EPR values with a rather low g_3 component were observed for Ru^{III} centers surrounded by three 2,4-dionato

(17) (a) Creutz, C. *Prog. Inorg. Chem.* **1983**, *30*, 1. (b) Demadis, K. D.; Hartshorn, C. M.; Meyer, T. J. *Chem. Rev.* **2001**, *101* 1655.

(18) (a) tom Dieck, H.; Franz, K.-D. *Angew. Chem.* **1975**, *87*, 244; *Angew. Chem., Int. Ed. Engl.* **1975**, *14*, 249. (b) Gardiner, M. G.; Lawrence, S. M.; Raston, C. L. *Inorg. Chem.* **1999**, *38*, 4467. (c) Cloke, F. G. N.; Dalby, C. I.; Henderson, M. J.; Hitchcock, P. B.; Kennard, C. H. L.; Lamb, R. N.; Raston, C. L. *J. Chem. Soc., Chem. Commun.* **1990**, 1394. (d) Rijnberg, E.; Boersma, J. T. B. H.; Jastrzebski, J.; Lakin, M. T.; Spek, A. L.; van Koten, G. *Organometallics* **1997**, *16*, 3158. (e) tom Dieck, H.; Kollvitz, W.; Kleinwächter, I. *Inorg. Chem.* **1984**, *23*, 2685. (f) Sieger, M.; Wanner, M.; Kaim, W.; Stufkens, D. J.; Snoeck, T. L.; Zalis, S. *Inorg. Chem.* **2003**, *42*, 3340.

(19) Ye, S.; Sarkar, B.; Lissner, F.; Schleid, T.; van Slageren, J.; Fiedler, J.; Kaim, W. *Angew. Chem.* **2005**, *117*, 2140; *Angew. Chem., Int. Ed.* **2005**, *44*, 2103.

Table 2. UV−vis−NIR Data of 1^n [$n = -2, -1, 0, +1, +2$] from Spectroelectrochemistry[a]

complex	λ_{max}/nm (ϵ/M^{-1} cm^{-1})
$\mathbf{1}^{2+}$	835(3400), 568(10 900), 445sh, 263(21 300)
$\mathbf{1}^{+}$	1795(2500), 822(10 500), 593sh, 448sh, 520(9100), 350sh, 277(21 800)
1	649(13 300), 600(12 500), 560sh, 450(9100), 341(13 400), 277(24 000)
$\mathbf{1}^{-}$	735(14 200), 549(8200), 413(8900), 347(11 200), 276(29 300)
$\mathbf{1}^{2-}$	828(13 800), 457(14 300), 322sh, 276(33 600)

[a] Measurements in CH_2Cl_2/0.1 M Bu_4NPF_6 (OTTLE spectroelectrochemistry).

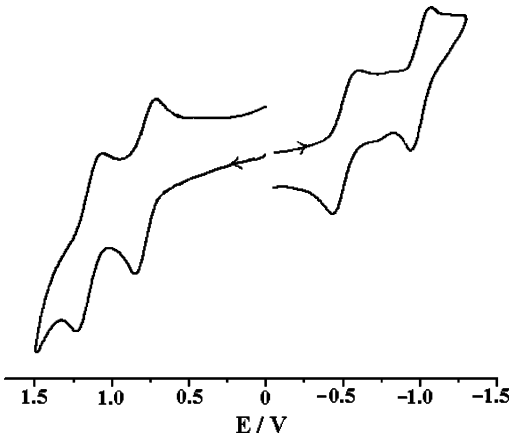

Figure 6. Cyclic voltammograms of **1** in CH_2Cl_2.

Scheme 1

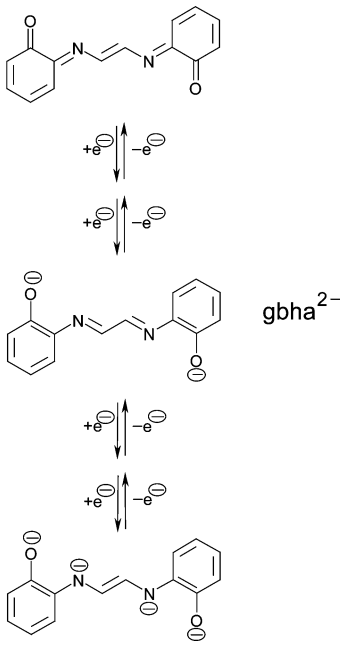

ligands of the acac$^-$ type.[20] The close-to-axial g tensor symmetry points to similar ligand field effects from acac$^-$ and the coordinated bridging ligand site, supporting the gbha$^{\bullet 3-}$ oxidation state with partially charged O and N donor atoms.

One-electron oxidation to $\{(\mu\text{-gbha})[Ru(acac)_2]_2\}^+$ ($\mathbf{1}^+$) produces significant spectral changes (Figure 5; Table 2). In addition to a bathochromically shifted charge-transfer transition, a broad band emerges in the NIR region at around

Scheme 2

$$[(acac)_2Ru^{IV}(gbha^{2-})Ru^{IV}(acac)_2]^{2+}$$
$$\overset{-e^-}{\underset{+e^-}{\rightleftharpoons}}$$
$$[(acac)_2Ru^{IV}(gbha^{2-})Ru^{III}(acac)_2]^{+}$$
$$\overset{-e^-}{\underset{+e^-}{\rightleftharpoons}}$$
$$[(acac)_2Ru^{III}(gbha^{2-})Ru^{III}(acac)_2]$$
$$\overset{-e^-}{\underset{+e^-}{\rightleftharpoons}}$$
$$[(acac)_2Ru^{III}(gbha^{\bullet 3-})Ru^{III}(acac)_2]^{-}$$
$$\overset{-e^-}{\underset{+e^-}{\rightleftharpoons}}$$
$$[(acac)_2Ru^{III}(gbha^{4-})Ru^{III}(acac)_2]^{2-}$$

1800 nm with a bandwidth at half-height of about $\Delta\nu_{1/2} = 2600$ cm^{-1} (Figure 5c). The second oxidation causes these features to disappear (Figure 5d); however, this last electron removal is not fully reversible on the longer time scale (ca. 1 min) of the spectroelectrochemistry experiment.

The NIR band is assigned to a typical IVCT transition (Figure 5c).[17] There have not been many clear cases reported where symmetrical Ru^{III}/Ru^{IV} complexes with d^4d^5 configuration exhibit such IVCT bands. Both higher[21] and lower[22] oxidation state combinations relative to the standard Ru^{II}/Ru^{III} situation[17] are rare. In some instances, the Ru^{III}/Ru^{IV} oxidation state assignment has been ambiguous [20] or the IVCT band could not be located with certainty.[21] Band analysis, according to Hush[23] [$\Delta\nu_{1/2}(\text{calcd}) = (2310\nu_{IVCT})^{1/2}$], yields a calculated bandwidth of 3580 cm^{-1}, somewhat higher than the experimental estimate of 2600 cm^{-1}.[17] Both the difference of the calculated and experimental values of $\Delta\nu_{1/2}$ and the K_c value of 10^6 suggest a valence-averaged formulation (class III[17]); however, a "borderline" situation,[17b] as that for the Creutz−Taube ion,[17] may also be considered.

The EPR measurements of $\{(\mu\text{-gbha})[Ru(acac)_2]_2\}^+$ support the assignment of a strongly coupled Ru^{III}/Ru^{IV} case, resulting from electron removal from metal-based orbitals (Figure 4). A relatively weak Ru^{III}-type signal is observed with $g_{1,2} = 2.220$ and $g_3 = 1.805$ ($g_{av} = 2.09$ and $\Delta g =$

(20) Hoshino, Y.; Higuchi, S.; Fiedler, J.; Su, C.-Y.; Knödler, A.; Schwederski, B.; Sarkar, B.; Hartmann, H.; Kaim, W. *Angew. Chem.* **2003**, *115*, 698; *Angew. Chem., Int. Ed.* **2003**, *42*, 674.

(21) (a) Patra, S.; Miller, T. A.; Sarkar, B.; Niemeyer, M.; Ward, M. D.; Lahiri, G. K. *Inorg. Chem.* **2003**, *42*, 4707. (b) Naklicki, M. L.; White, C. A.; Kondratiev, V. V.; Crutchley, R. J. *Inorg. Chim. Acta* **1996**, *242*, 63. (c) Patra, S.; Sarkar, B.; Maji, S.; Fiedler, J.; Urbanos, F. A.; Jimenez-Aparicio, R.; Kaim, W.; Lahiri, G. K. *Chem. Eur. J.* in print.

(22) Sarkar, B.; Kaim, W.; Fiedler, J.; Duboc, C. *J. Am. Chem. Soc.* **2004**, *126*, 14706.

(23) Hush, N. S. *Prog. Inorg. Chem.* **1967**, *8*, 391.

0.41) (Figure 2c), which is more intense at 110 K than at 4 K. The similarity of *g* positions and EPR appearance (Figure 2) for $\mathbf{1}^+$, **1**, and $\mathbf{1}^-$ is not unexpected, given the relatively unchanged ligand field and Ru^{III} metal configuration. The possibility of singlet or triplet states for Ru^{IV} coupled with Ru^{III} creates opportunities for rapid EPR relaxation, which diminishes the signal intensity for $\mathbf{1}^+$. In fact, the related system $\{(\mu\text{-boptz})[Ru(acac)_2]_2\}^+$, $bpotz^{2-}$ = 3,6-bis(2-oxidophenyl)-1,2,4,5−tetrazine, is EPR silent[21c] because of a weaker metal−metal coupling in the mixed-valent state; this interpretation is supported by the absence of a detectable IVCT band and by a lower K_c value of 7.9×10^3.[21c]

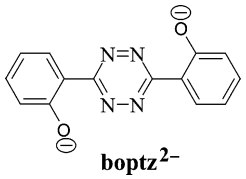

boptz^{2-}

The reason for this pronounced difference can be found in the probable mechanism of valence exchange. The high oxidation states Ru^{III} and Ru^{IV} require a hole transfer mechanism[24] to operate; that is, a high-lying π MO should be available for mediating the valence exchange between the two metal centers. In the present case, this π MO is dominated by the two phenolate groups which, however, are coupled in a very different way, either by the C atoms of the weakly basic six-center tetrazine ring in $boptz^{2-}$ or by the more basic N atoms of the smaller (four-center) 1,4-diazabutadiene connector in $gbha^{2-}$. Clearly, the latter can provide a more efficient π interaction of the phenolates and, thus, of the metal centers.

In summary, we have not only shown a new unprecedented bridging coordination mode for the π-conjugated dianion $gbha^{2-}$, derived from the well-established photometric reagent glyoxalbis(2-hydroxyanil), we have also established the noninnocence of this 1,4-diazabutadiene ligand in terms of its stepwise reversible reduction and its capacity to stabilize the less-common Ru^{III}/Ru^{IV} mixed-valent state because of metal coordination by five negatively charged oxygen atoms. That state could be analyzed by EPR and UV−vis−NIR spectroscopy, including the identification of an intervalence charge-transfer band at 1800 nm; the data, in conjunction with the comproportionation constant of about 10^6, suggest a valence-averaged $(Ru^{3.5})_2$ formulation (class III) with a tendency toward class II ("borderline" situation[17b]).

While our assignments, based on spectroscopic evidences, are considered plausible and consistent, a recent sophisticated theoretical approach to the electronic structure of even simpler mononuclear ruthenium complexes with redox-active quinonoid ligands (see Patra et al.[10]) has illustrated the complexity of such systems (see Kaupp and Remenyi[25]), which may require a very-high-level theoretical analysis for a full understanding.

Experimental Section

The precursor compound $Ru(acac)_2(CH_3CN)_2$[26] was prepared according to a reported procedure. The ligand glyoxalbis(2-hydroxyanil) (H_2gbha) was purchased from Aldrich. Other chemicals and solvents were reagent grade and were used as received. For spectroscopic and electrochemical studies, HPLC grade solvents were used.

UV−vis−NIR spectroelectrochemical studies were performed in CH_3CN/0.1 M Bu_4NPF_6 at 298 K using an OTTLE cell[16] mounted in the optical path of a J&M Tidas spectrophotometer by means of an adapted sample holder. FT-IR spectra were taken on a Nicolet spectrophotometer with samples prepared as KBr pellets. Solution electrical conductivity was checked using a Systronic 305 conductivity bridge. The EPR measurements were made in a two-electrode capillary tube[27] with an X-band Bruker system ESP300, equipped with a Bruker ER035M gaussmeter and a HP 5350B microwave counter. Electrochemistry experiments were carried out using a PAR model 273A electrochemistry system. Platinum wire working and auxiliary electrodes and an aqueous SCE were used in a three-electrode configuration. The supporting electrolyte was 0.1 M NEt_4ClO_4, and the solute concentration was $\sim 10^{-3}$ M. The half-wave potential $E_{298}°$ was set equal to $0.5(E_{pa} + E_{pc})$, where E_{pa} and E_{pc} are the anodic and cathodic cyclic voltammetric peak potentials, respectively. A platinum wire-gauze working electrode was used in the coulometric experiments. The elemental analyses were carried out with a Perkin-Elmer 240C elemental analyzer. Electrospray mass spectra were recorded on a Micromass Q-ToF mass spectrometer.

Synthesis of $(acac)_2Ru^{III}(\mu\text{-gbha})Ru^{III}(acac)_2$ (1). The starting complex $Ru(acac)_2(CH_3CN)_2$ (100 mg, 0.26 mmol), the ligand H_2gbha (31 mg, 0.13 mmol), and sodium acetate (22 mg, 0.26 mmol) were dissolved in 20 mL of ethanol, and the mixture was heated to reflux for 8 h. The initially orange solution gradually changed to blue. The solvent of the reaction mixture was evaporated to dryness under reduced pressure, and the residue was then purified using a neutral alumina column. Initially, a red compound corresponding to $Ru(acac)_3$ was eluted by CH_2Cl_2, followed by blue **1**, eluted with $CH_2Cl_2-CH_3CN$ (25:1). Evaporation of the solvent under reduced pressure yielded the pure complex **1**. Yield: 56 mg (51%). Anal. Calcd (found): C, 48.80 (48.62); H, 4.58 (4.87); N, 3.35 (3.18).

Magnetic Measurements. The variable-temperature magnetic susceptibility data were measured on a Quantum Design MPMSXL SQUID (Superconducting Quantum Interference Device) susceptometer over a temperature range of 2−300 K. Data were corrected for diamagnetic contributions to the total susceptibility from the sample holder and the complex. The molar diamagnetic corrections were calculated on the basis of Pascal constants. The fitting of the experimental data was carried out using the commercial MATLAB V.5.1.0.421 program.

Computational Details. Full geometry optimization was carried out using the density functional theory method at the (U)B3LYP level.[28a,b] All elements except ruthenium were assigned the 6-31G* basis set. The SDD basis set with an effective core potential was employed for the ruthenium atoms.[28c,d] Calculations were performed with Gaussian98.[28e] Vertical electronic excitations based on B3LYP optimized geometries were computed using the TD-DFT formalism[28f] with the B3LYP functional using the above combination of basis

(24) (a) Kaim, W.; Klein, A.; Glöckle, M. *Acc. Chem. Res.* **2000**, *33*, 755. (b) Crutchley, R. J. *Adv. Inorg. Chem.* **1994**, *41*, 273.
(25) Remenyi, C.; Kaupp, M. *J. Am. Chem. Soc.* **2005**, *127*, 11399.
(26) Kobayashi, T.; Nishina, Y.; Shimizu, K. G.; Satô, G. P. *Chem. Lett.* **1988**, 1137.
(27) Kaim, W.; Ernst, S.; Kasack, V. *J. Am. Chem. Soc.* **1990**, *112*, 173.

sets. A visual inspection of all key orbitals was done with MOLDEN[28g] to assign the nature of various electronic transitions.

Acknowledgment. Financial support received from the Department of Science and Technology, Council of Scientific and Industrial Research (India), the DAAD, and the DFG (Germany) is gratefully acknowledged.

Supporting Information Available: Selected list of optimized bond lengths, bond angles, and torsional angles for the triplet ground state of **1** at the B3LYP/SDD,6-31G* level (Table S1); optimized bond lengths, bond angles, and torsional angles for the lowest state of singlet **1** at the B3LYP/SDD,6-31G* level (Table S2); list of vertical excitations computed at the TD-DFT/B3LYP//B3LYP/SDD,6-31G* level for triplet of **1** (Table S3); coordinates of optimized triplet and singlet ground states of **1** and free $gbha^{2-}$ at the B3LYP/SDD,6-31G* and B3LYP/6−31G* levels, respectively (Table S4); temperature dependence of the magnetic susceptibility χ_M and of the magnetic moment μ_{eff} for **1** (Figure S1); optimized structure of singlet **1** (Figure S2); Kohn−Sham orbital contours of the orbitals involved in the key transitions of **1** in triplet state (Figure S3). This material is available free of charge via the Internet at http://pubs.acs.org.

IC050950R

(28) (a) Becke, A. D. *Phys. Rev. A* **1988**, *38*, 3098. (b) Lee, C.; Yang, W.; Parr, R. G. *Phys. Rev. B* **1988**, *37*, 785. (c) Andrae, D.; Haeussermann, U.; Dolg, M.; Stoll, H.; Preuss, H. *Theor. Chim. Acta* **1990**, *77*, 123. (d) Fuentealba, P.; Preuss, H.; Stoll, H.; Szentpaly, L. V. *Chem. Phys. Lett.* **1989**, *89*, 418. (e) Frisch, M. J.; Trucks, G. W.; Schlegel, H. B.; Scuseria, G. E.; Robb, M. A.; Cheeseman, J. R.; Zakrzewski, V. G.; Montgomery, J. A., Jr.; Stratmann, R. E.; Burant, J. C.; Dapprich, S.; Millam, J. M.; Daniels, A. D.; Kudin, K. N.; Strain, M. C.; Farkas, O.; Tomasi, J.; Barone, V.; Cossi, M.; Cammi, R.; Mennucci, B.; Pomelli, C.; Adamo, C.; Clifford, S.; Ochterski, J.; Petersson, G. A.; Ayala, P. Y.; Cui, Q.; Morokuma, K.; Malick, D. K.; Rabuck, A. D.; Raghavachari, K.; Foresman, J. B.; Cioslowski, J.; Ortiz, J. V.; Stefanov, B. B.; Liu, G.; Liashenko, A.; Piskorz, P.; Komaromi, I.; Gomperts, R; Martin, R. L.; Fox, D. J.; Keith, T.; Al-Laham, M. A.; Peng, C. Y.; Nanayakkara, A.; Gonzalez, C.; Challacombe, M.; Gill, P. M. W.; Johnson, B.; Chen, W.; Wong, M. W.; Andres, J. L.; Gonzalez, C.; Head-Gordon, M.; Replogle, E. S.; Pople, J. A. *Gaussian 98*, revision A.6; Gaussian, Inc.: Pittsburgh, PA, 1998. (f) Casida, M. In *Recent Advances in Density Functional Methods*; Chong, D. P., Ed.; World Scientific Press: Singapore, 1995; Vol. I, p 155. (g) Schaftenaar, G.; Noordik, J. H. *J. Comput.-Aided Mol. Design*, **2000**, *14*, 123.